Journal of applied research and technology
ISSN: 1665-6423
Universidad Nacional Autónoma de México, Instituto de Ciencias Aplicadas y Tecnología

Prince, R. Malkiya Rasalin; Selvakumar, N.; Arulkirubakaran, D.; Ezhil Singh, S. Christopher; Das, M. Chrispin; Prabha, C.; Bannaravuri, Praveen Kumar; Robert, R. B. Jeen; Prephet, I. Living

TG/DTA studies on the oxidation and thermal behaviour of Ti-6Al-4V-B4C coatings obtained by magnetron sputtering

Journal of applied research and technology, vol. 18, no. 3, 2020, pp. 178-186
Universidad Nacional Autónoma de México, Instituto de Ciencias Aplicadas y Tecnología

DOI: https://doi.org/10.14482/INDES.30.1.303.661

Journal of Applied Research and Technology

www.jart.icat.unam.mx

Journal of Applied Research and Technology 18 (2020) 108-118

Original

TG/DTA studies on the oxidation and thermal behaviour of Ti-6Al-4V-B_4C coatings obtained by magnetron sputtering

R. Malkiya Rasalin Prince[a]* • N. Selvakumar[b] • D. Arulkirubakaran[a] • S. Christopher Ezhil Singh[c] • M. Chrispin Das[d] • C. Prabha[c] • Praveen Kumar Bannaravuri[a] • R. B. Jeen Robert[e] • I. Living Prephet[f]

[a]*Department of Mechanical Engineering, Karunya Institute of Technology and Sciences, Coimbatore - 641114, Tamilnadu, India*
[b]*Department of Mechanical Engineering, Mepco Schlenk Engineering College, Sivakasi 626 005, Tamil Nadu, India*
[c]*Department of Mechanical Engineering, Vimal Jyothi Engineering College, Chemperi, Kannur 670632, Kerala, India*
[d]*Department of Mechanical Engineering, St Joseph's Institute of Technology, Chennai - 600119, Tamilnadu, India*
[e]*Department of Mechanical Engineering, AAA College of Engineering and Technology, Sivakasi - 626123, Tamilnadu, India*
[f]*Department of Mechanical Engineering, Bethlahem Institute of Engineering, Karungal, Tamilnadu, India*

Received 03 12 2020; accepted 05 11 2020
Available online 06 30 2020

Abstract: Thermogravimetric analysis (TG) is a rapid method for the determination of protecting the ability of thin film coatings in addition to oxidation kinetics. Boron carbide (B_4C) reinforced Ti-6Al-4V thin films were deposited through the magnetron sputtering coating technique. The effect of 0, 2, 4, 6 and 8 Wt. % of B_4C adding on microstructure, thermal behaviour and hardness of Ti-6Al-4V-B_4C coatings were investigated. Thermal analysis of Ti-6Al-4V-B_4C coatings with varying percentage of B_4C resulted in the establishment of an exothermic peak, for the reason that reduction in the oxidation of coating. The thermal behaviour of coating was improved by B_4C addition; those coatings are recommended for practical application. It was proven that the addition of B_4C not only alters the thermal stability but also transforms the mechanism of oxidation. It was absolutely unconcealed that the Ti-6Al-4V-B_4C film oxidization may be a multi-staged procedure subject on the heating rate. An occurrence of formal treatment for obtaining Kissinger's assessment mechanics for various oxidization levels is additionally valid. The addition of B_4C was supported to enhance the nanohardness of the coating. The morphology, composition and structure of the thin film coatings were examined by way of SEM, AFM and XRD.

Keywords: Thermogravimetric analysis, differential thermal analysis, oxidation kinetics, activation energy, nanohardness

*Corresponding author.
E-mail address: russelmecher@gmail.com (R. Malkiya Rasalin Prince).
Peer Review under the responsibility of Universidad Nacional Autónoma de México.

1. Introduction

Thermally stabled thin film coatings are commonly used as a protection shield for hot gas turbine engine parts by dropping the metal substrate temperatures (Padture, Gell & Jordan, 2002). According to the literature, typical ceramic coatings are applied to provide thermal insulation of engineering components. In order to develop the sturdiness and efficiency of gas turbine engines, it is essential to create a substitute ceramic coating appropriate for applications more than 1000°C (Belmonte, 2006; Stecura, 1986). In such a way that the physical vapor deposition (PVD) technique has been used for the deposition of hard thin film coatings (Yang, Cho, & Lin, 2014). Also, magnetron sputtering is a common technique to produce thin film coatings with better quality because it is unnecessary a post-deposition treatement (Selvakumar & Prince, 2017). However, the surface engineering arena is mainly focused on carbides and nitrides-based coatings because of its extraordinary hardness (Robinson & Jackson, 2005).

A high sensitive TG/DTA analysis was employed to analyze the thermal behaviour of thin-film coatings. Also, the addition of boron carbide particles enhanced the thermal stability (Polyakova & Hübert, 2001). The mass loss of Al-TiC nanocomposites happened for the period of decomposition of nanoparticles and the particle size variation of TiC affects the conversion of enthalpy. (Selvakumar, Sivaraj, & Muthuraman, 2016) discussed weight gain due to the micron size particle by DSC analysis and weight gain was identified at 825°C. (Azhagurajan, Selvakumar, & Mohammed Yasin, 2012) reported that nanoparticles expose superior thermal behaviour than micron-sized particles. Moreover, high thermal energy was created by nanosized aluminium powder. Nanoindentation procedure is universally used for calculating nanohardness of the thin film coatings. Mechanical properties of various coatings can be analyzed by the AFM nanoindentation technique (An, Wen, Hu, Tian, & Zheng, 2008). The present work focuses on investigating the thermal behaviour of Ti-6Al-4V-B_4C thin film coatings with varying B_4C content. Ti-6Al-4V-xB_4C thin film coatings with different compositions (x= 0, 2, 4, 6 and 8) were prepared using the magnetron sputtering method. The impact of the B4C content addition on the microstructure, thermal behaviour and nanohardness of the coatings was inspected.

2. Investigations

The process flow diagram of the experimental study is shown in Fig. 1.

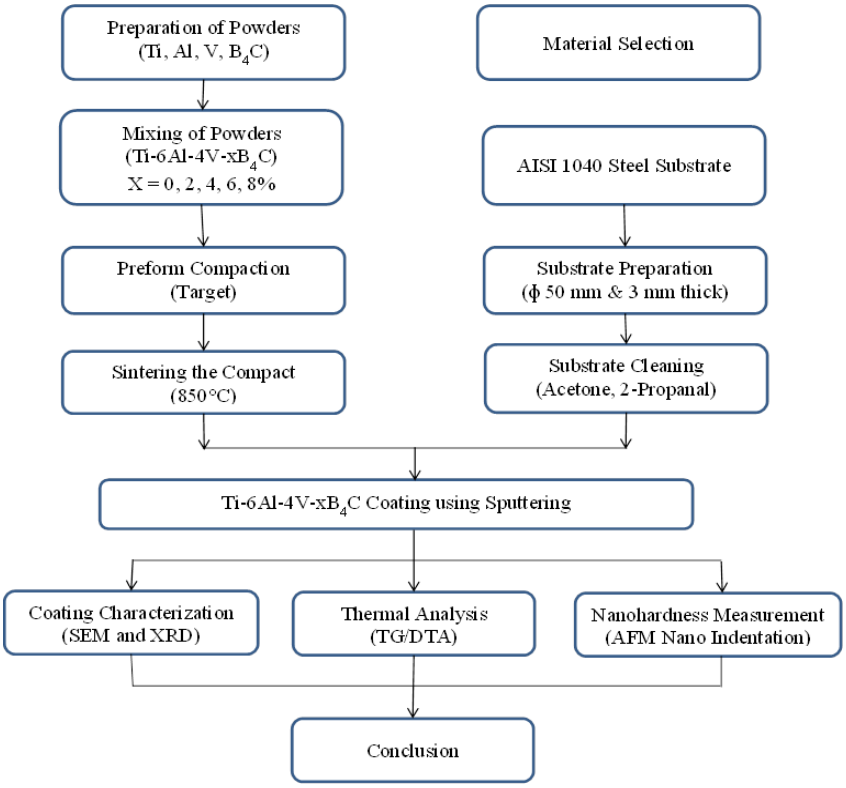

Figure 1. Process flow diagram.

2.1. Materials

Mechanical properties of Ti-6Al-4V titanium alloy have higher at normal atmospheric temperatures. B_4C is an immensely unbreakable ceramic in addition to standing third behind the precious stone as well as cubic boron nitride. The powders Ti, Al, V and B_4C supplied by M/s. Sigma Aldrich (India) were used as a target material. AISI 1040 steel plates were purchased from M/s. steel mart Mumbai.

2.2. Preparation of the thin film

The starting materials used for preparing targets are Ti, Al, V and B_4C with a particle size <5 µm. The target of a 50 mm diameter with 3 mm thickness was produced through vacuum condition under a uniaxial load of 750 *MPa* at room temperature. The prepared target particle size of 0.5–5 *µm* was observed with irregular and angular shapes were obtained by SEM and shown in Fig. 2. The mirror-polished AISI 1040 was used as a substrate for coating with measurements of 50 *mm* diameter and *3 mm* thickness.

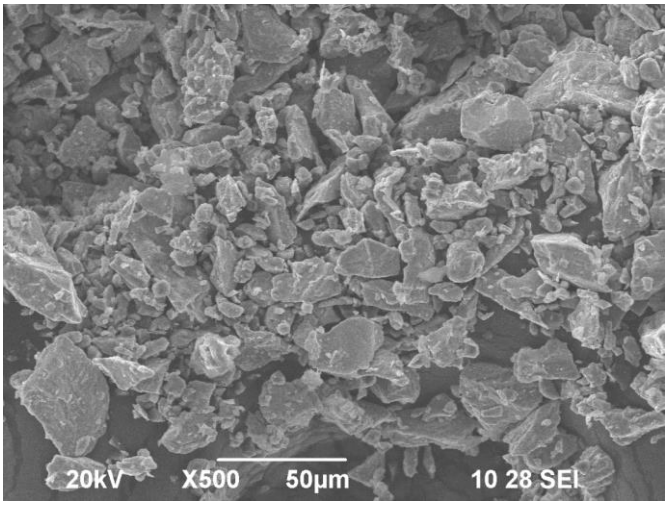

Figure 2. SEM image of precompacted Ti-6Al-4V-8B4C powders.

2.3. Characterization of the thin films

The XPERT-PRO diffractometer was used to analyze the crystalline structure of the coating. A Cu Kα radiation (k = 1.54060 Å) was utilized, 2θ range of 10–80° with 30 *kV* and 30 *mA* was used. Nanohardness of the coating was executed by AFM XE-70, Park Systems made by South Korea through the AFM nanoindentation technique.

2.4. Procedure of TG/DTA study

Ti-6Al-4V-B_4C thin films were inspected through Differential Thermal Analysis (DTA) and Thermo Gravimetric Analysis (TG) in the air by SIINT 6300 analyzer, (Japan). An approximately 10 *mg* of Ti-6Al-4V-B_4C coated thin film isolated samples (2x2*mm*) were heated up to 1000°C with a heating rate of 10°C/min under atmospheric air in an open platinum crucible. An amendment of mass with respect to temperature was resolute and brought as a mass changing rate (TG curve) for comparison against DTA curves. DTA curve signifies that heat flow variations throughout heating by way of physical transformations furthermore as chemical reactions within the sample. The melting, crystallization and ignition behaviour of Ti-6Al-4V-B_4C thin film was investigated by using DTA. Equation (1) (Lin, Mishra, Moore, & Sproul, 2008) describes the relationship between the highest temperature T_m of the exothermic oxidation reaction and activation energy of Ti-6Al-4V- B_4C thin film.

$$\mathrm{Ln}\left(\frac{\emptyset}{T_m^2}\right) = -\frac{E_a}{kT_m} + constant \quad (1)$$

Where k = gas constant (eVK^{-1}), φ = heating rate (Ks^{-1}), T_m = exothermic oxidation reaction peak temperature (K), E_a= activation energy (eV $atom^{-1}$)

3. Results and discussion

3.1. XRD analysis

XRD peaks of 8% B_4C reinforced Ti-6Al-4V is shown in Figure 3. Various elements present in the coating was confirmed through elements peaks; Ti peaks represented by high-intensity peaks with 2θ values of 35.1°, 40.2°, 62.9°, 70.6°, 76.1° and 77.3° fit into the crystal planes of (1 0 0), (1 0 1), (1 1 0), (1 0 3), (1 1 2) and (2 0 1) are authenticate by JCPDS 89-2762. Also, another element of Aluminium was acknowledged by different peaks with 2θ values of 38.4°, 44.8° and 78.3° through (1 1 1), (2 0 0) and (3 1 1) planes authenticate by JCPDS file no 89-4037. Vanadium peak is identified at (1 1 0) plane with a 2θ angle of 41.2° and authenticate by JCPDS file no 65-6689. The 2θ values of 53.4°, 58.8° and 65.1° through (2 0 0), (2 1 4) and (0 2 7) planes have confirmed the presence of Boron carbide and authenticate by JCPDS file No 75-0424. Based on the presence of different peaks present in the coating it is confirmed that no oxide peak is identified in the coating. Moreover, XRD patterns authenticate the presence of B_4C in the coating. The size of the particles in the coatings is in nanosized; confirms by peak width.

3.2. Thermal studies

Fig. 4 (a-e) describes the thermal behaviour (TG/DTA) of Ti-6Al-4V B_4C coating with 0, 2, 4, 6 and 8% B_4C. Thermogravimetric and differential thermal analysis (TG/DTA) techniques were enforced to compute the thermal stability of the Ti-6Al-4V- B_4C thin films at under normal temperature and atmospheric air. The weight loss of the Ti-6Al-4V-B_4C thin films was noticed. Average volatility before melting and melting point of all Ti-6Al-4V-B_4C thin films was mentioned. DLC films were entirely wrecked over 500°C, representing the evaporation of the pure

DLC films reported by having, Xianghui and Shuichi (2013). Conversely, up to 650°C the Ti-6Al-4V- B_4C films were stable; moreover (Chavin et al., 2013) reported that during heating around 600°C the diamond-like carbon coating was disappeared.

In the present study, all the Ti-6Al-4V- B_4C thin films were heated to 1000°C. The weight loss of the pure Ti-6Al-4V- B_4C film considerably decreased at temperatures up to 500°C. In film considerably decreased at temperatures up to 500°C. In addition, the Ti-6Al-4V- B_4C thin films are of little volatile nature and weight gain was gradually increased above 500°C temperature because of the presence of oxygen contents. Then, the Ti-6Al-4V-0B_4C films wiped out while heated above 650°C and were not thermally stable when heated over 650°C. At the time of heating, the Ti-6Al-4V-0B_4C films gained weight and the adsorption of oxygen content from the atmospheric air was identified (Chavin et al., 2013).

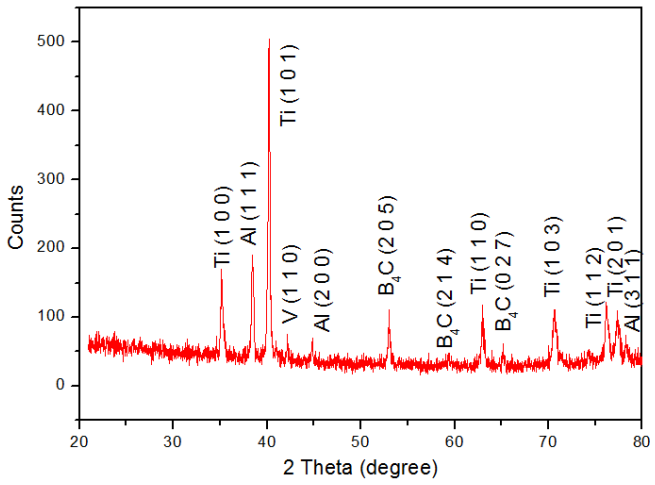

Figure 3. XRD of coating.

An increase in the ignition temperature was noticed in the coating because of the presence of B_4C and changes in thermal behaviour were also observed. According to the results obtained by DTA studies, the effective values of activation energy were calculated for the isothermal reduction stage for the Ti-6Al-4V-2B_4C thin film. The substantial thermal response peaks of Ti-6Al-4V-4B_4C thin film were in the DTA curve as mentioned in Fig. 4 (c). The peak temperatures of Ti-6Al-4V-4B_4C thin films were noted from the first derivative DTA curve. A DTA analysis of the Ti-6Al-4V-4B_4C deposited film was fulfilled to recognize the structural in addition to phase changes rise in the DTA curve.

In Fig. 4 (c), the deposited Ti-6Al-4V-4B_4C film encloses an amalgamation of dual phases, a bulky amount of hexagonal (Ti) phase with (1 0 1), (1 1 0), (1 0 3) and (1 1 2) orientations in addition to a small fraction of face center cubic B_4C phase with (2 0 0), (2 1 4) and (0 2 7) orientation, that confirms the sub-stoichiometric concentration in this film. At the beginning, two exothermal peaks occurred at 325°C and 650°C, which are shown in Fig. 4 (c). The mass loss was disclosed within the TG curve in the middle of 830°C and 900°C, presenting the best decomposition phase of Ti-6Al-4V-4B_4C films. The combined DTA as well as TG investigation exposed that the Ti-6Al-4V-4 B_4C film was oxidized at 600°C, which matches the onset of the weight increase within the TG curve, and therefore the main oxidation temperature was at 940°C. However, it was observed that oxygen concentration will play a dynamic character in deciding the Ti-6Al-4V-4B_4C film's oxidation behaviour.

It was noted that the mass loss took place at around 425 °C and was completed at around 850 °C. The thermal stability of B_4C had more than Al because B_4C had a complex crystal structure. Thus, the complex crystal structure of B_4C particles changed the ignition temperature finally the ignition temperature was increased and the thermal behaviour of the coating also increased. The slower rate of decomposition was observed in the Ti-6Al-4V-6 B_4C thin film and it is mentioned in Fig. 4 (d). In general, the presence of oxygen particles in the atmosphere may react with Al and produces aluminium oxide film which is stable and securely adhering. But at the time of heating, the aluminium oxide film may decompose. This is depicted in Fig. 4 (e) which shows 0.1% and/or 0.2% loss in weight. This property becomes modified by the addition of reinforcements (Selvakumar & Vettivel, 2013).

3.3. Oxidation behaviour of the coating

Fig. 4 (a) points out the sample progressed with a weight loss up to 825°C additional stable weight gain is achieved up to 998.6°C within the Ti-6Al-4V- B_4C coating as well as Fig. 4 (b) point out weight loss progressed with a smaller amount of weight gain. Weight gain is expected by the oxidation reaction of a coating with nearby atmosphere air. The non-isothermal oxidation of thin films by heating to 1000°C at a rate of 10°C min^{-1} is signified by alpha (α) value as a function of temperature (T). A further value of α was attained by means of dividing the observed weight gain by the theoretical observed weight gain evaluated based on Eq. (2).

$$Ti + O_2 \rightarrow TiO_2 \quad (2)$$

Oxidation nature of samples provides nearly a similar initiation temperature of approximately 550°C, but not the same oxidation temperatures; it varies subject to the coating composition. The sample is heated up to 1000 °C. In α-T curves with the lower amount of carbon content (2% B_4C) give an oxidation point at around α = 25%, in contrast to those with a better quantity of carbon content that provides around α = 40–50%. Initially, a slower oxidation rate is perceived, subsequently proceeds rapid oxidation due to an increase in temperature rise.

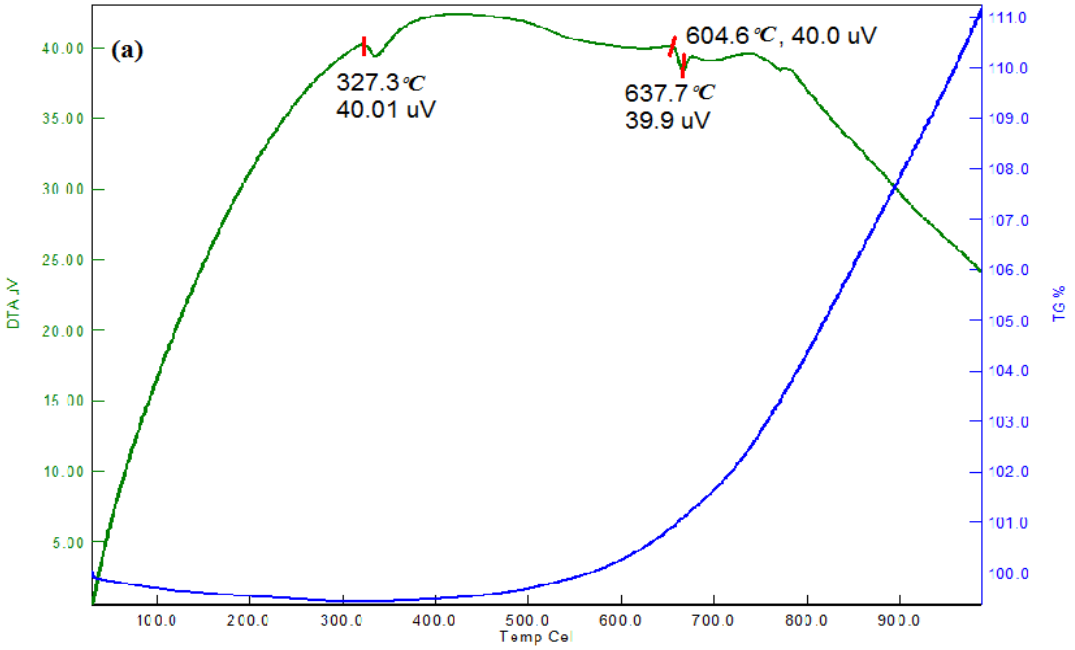
(a)
327.3℃
40.01 uV
604.6℃, 40.0 uV
637.7℃
39.9 uV
DTA uV
TG %
Temp Cel

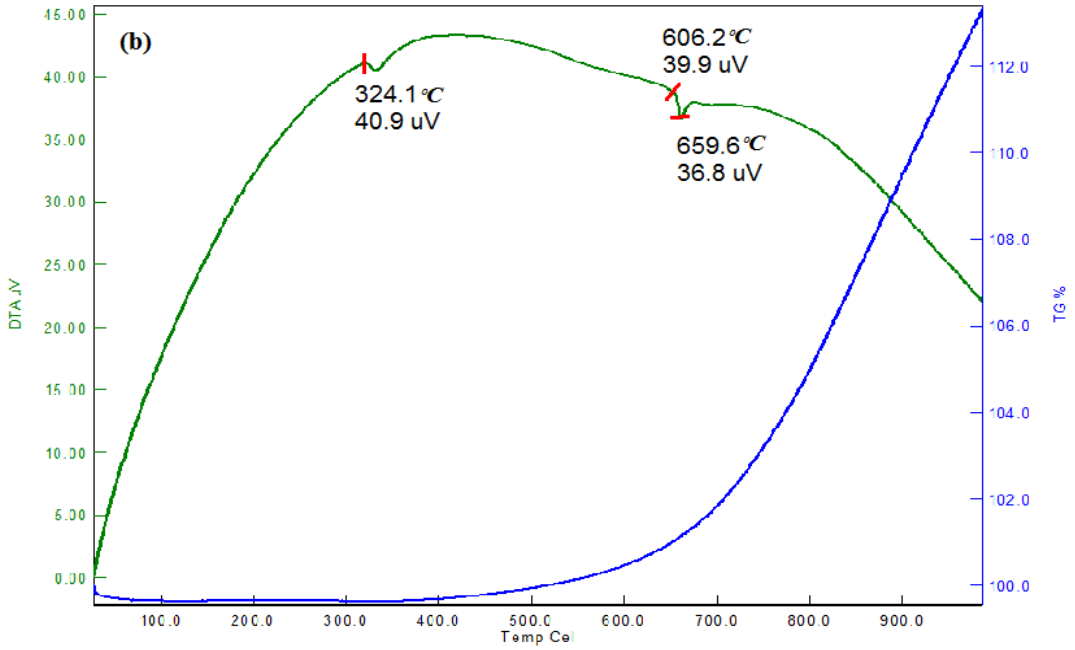
(b)
324.1℃
40.9 uV
606.2℃
39.9 uV
659.6℃
36.8 uV
DTA uV
TG %
Temp Cel

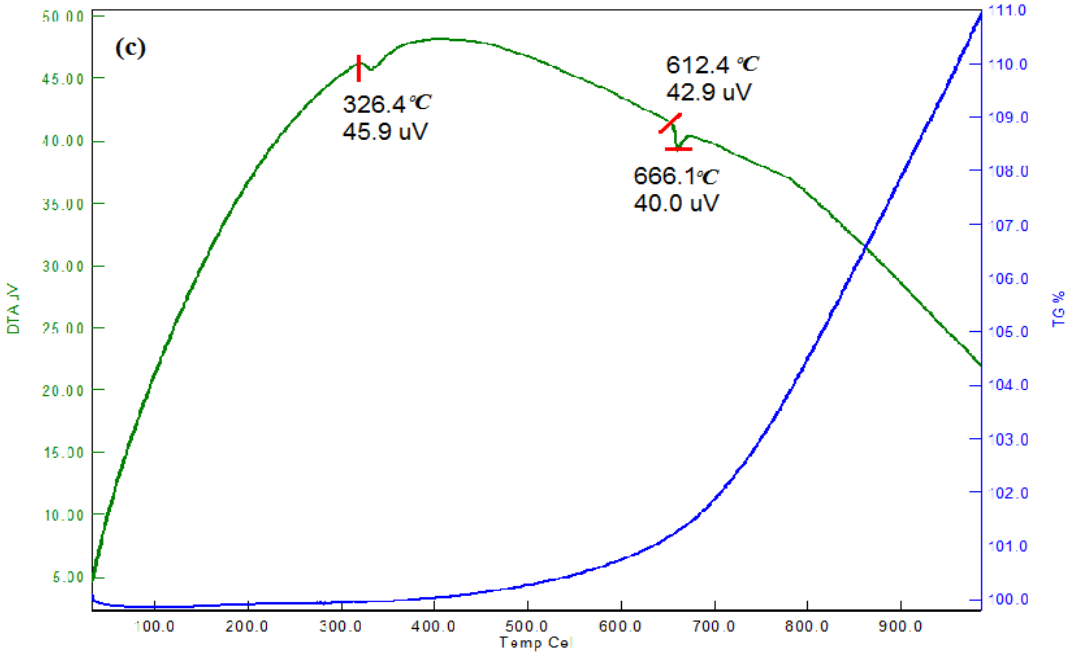
(c)
326.4℃
45.9 uV
612.4 ℃
42.9 uV
666.1℃
40.0 uV
DTA uV
TG %
Temp Cel

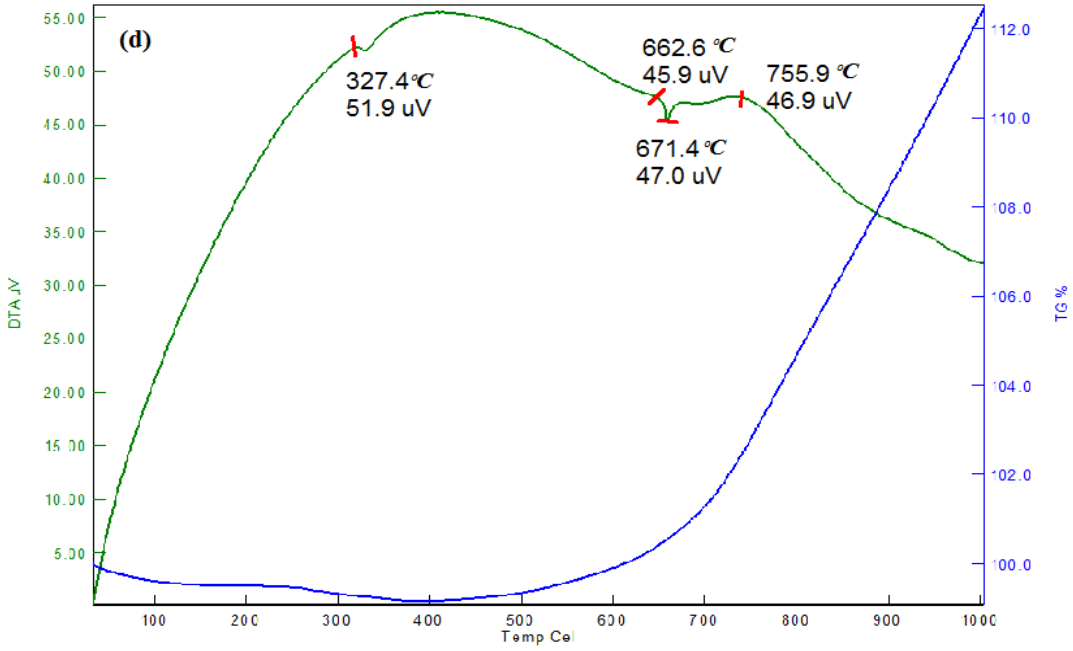
(d)
327.4℃
51.9 uV
662.6 ℃
45.9 uV
755.9 ℃
46.9 uV
671.4℃
47.0 uV
DTA uV
TG %
Temp Cel

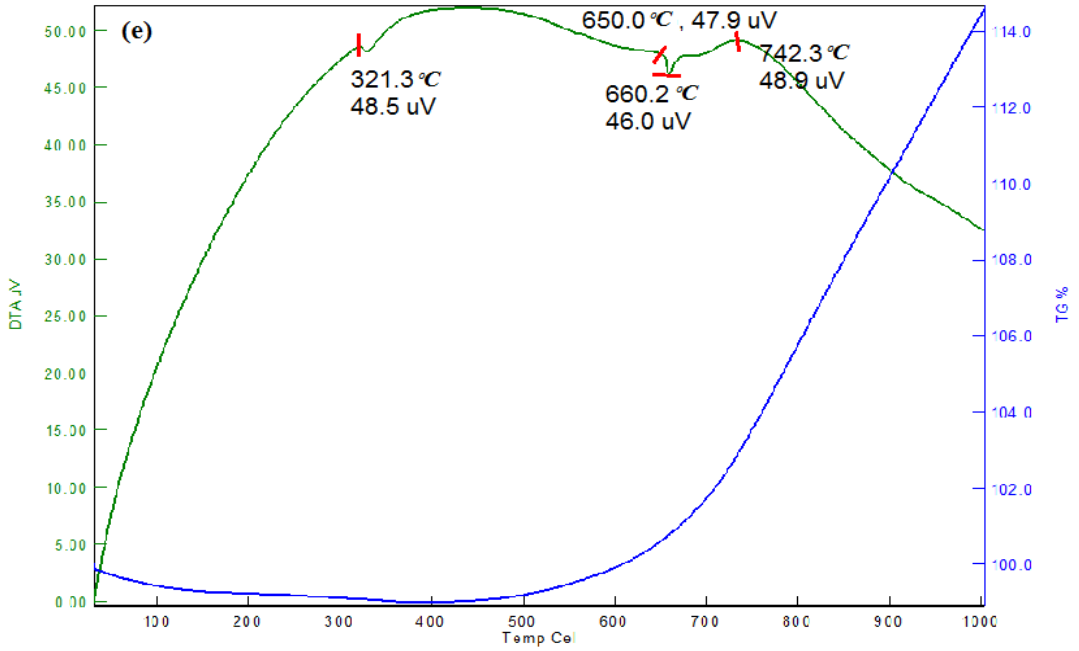

Figure 4. Thermal analysis for Ti-6Al-4V-xB_4C coatings with different B_4C (%) (a) x=0, (b) x=2, (c) x=4, (d) x=6, I x=8.

The thermal changes created by oxidation of Ti-6Al-4V B_4C thin film are illustrated in Fig. 4 (a) by DTA curves. All examples were anticipated with an exothermic peak; the oxidation of Ti-6Al-4V-B_4C thin film generates two overlying exothermic peaks. In this manner, the exothermic changes happen gradually, a while later a steep rise in temperature reported by Prince et al. (2020).

The isothermal oxidation behaviour of thin-film samples was performed at 745°C up to 2000 s and is shown in Fig. 5. The oxidation rate turns out to be faster in the order of 8% B_4C > 6% B_4C > 4% B_4C > 2% B_4C > 0% B_4C in agreement with the non-isothermal TG as well as DTA results. Also, the peak oxidation rate due to the presence of carbon content in the form of B_4C and the oxidation rate is controlled by B4C particles. The oxidation of Ti-6Al-4V-B_4C coating is also matched according to the thermodynamic data (ΔG) of the succeeding Equations (3-5).

$$Al + O_2 = Al_2O_3 \quad (3)$$

$$V + O_2 = V_2O_5 \quad (4)$$

$$B_4C + O_2 \rightarrow B_2O_3 + CO_2 \quad (5)$$

The ΔG values for reactions 3 and 4 in an exceeding temperature vary of 500–C - 800°C and resembling one another. Thus, the ease of oxidation of Ti-6Al-4V- B_4C coating in the above order cannot be delineated by the thermodynamic data then again it could be determined by a kinetic factor. The oxidation kinetics for Ti-6Al-4V-xB_4C coating is delineated by a diffusion-limited reaction, signified in the Jander equation (Shimada, Johnsson, & Urbonaite, 2004) (6):

$$K_{Jt} = \left[1 - (1-\propto)^{1/3}\right]^2 \quad (6)$$

Where K_J is the Jander rate constant and t is the time. On the other hand, it seems that the oxidation of the Ti-6Al-4V-x B_4C coating process according to the first-order rate equation (7).

$$K_{Ft} = -\ln(1-\alpha) \quad (7)$$

where k is the first-order rate constant. Eq. (7) is standard for the reason that the nucleation and growth kinetic equation. The oxidation of Ti-6Al-4V-x B_4C coating was rapid in the primary stage (<200 s) that it was not judged. It is distinguished that the lower oxidation temperature of Ti-6Al-4V-xB_4C coating at 700°C is imported by way of the first-order rate equation, on the other hand, higher temperature oxidation (790 and 900°C) is signified by the diffusion-limited Jander equation. The thermal alterations progressed in the initial oxidation (<2000 s) were monitored in all the samples, as presented in Fig. 5, which reported that the zero time for oxidation is shifted to every 200 s due to the increase in carbon content in the coating.

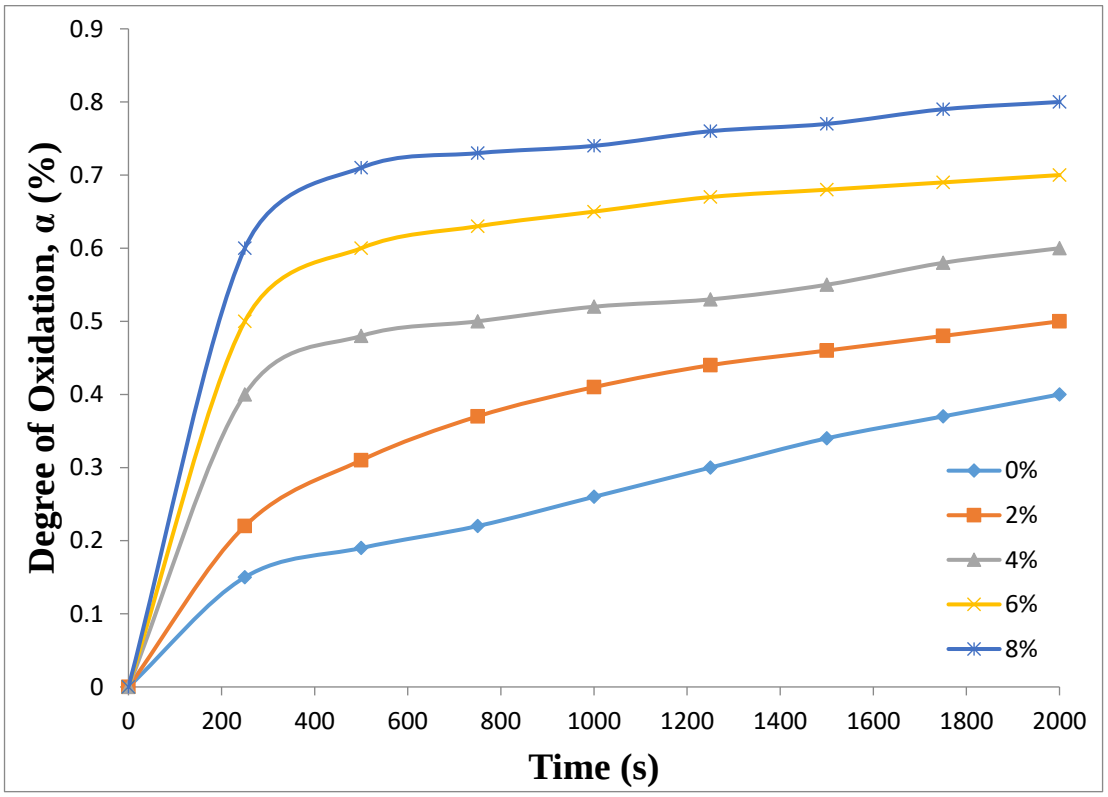

Figure 5. Isothermal oxidation of the Ti-6Al-4V-XB$_4$C thin film.

A large exothermic effect appears in the very early oxidation stage <500 s, trailed by slower heat evolution. The isothermal oxidation of all conformations was accomplished at a higher temperature around 850°C. It is concluded that the oxidation of Ti-6Al-4V-B$_4$C coating generates the mass gain that shows within the DTA curves.

A minor weight loss of 1.2 wt.% was noted in the primary stage at temperatures not up to 280°C in TG curve could also be as a result of adsorbed gases in addition to water particle on the sample, for the reason that this weight decrease altered by the heating of the sample at 110°C in the TG/DTA curve. Afterward, a weight gain increase due to the oxidation starts at temperatures beyond 625°C. Once the weight gain starts, in contrast with a Ti-6Al-4V-xB$_4$C coating, it is monitored that a quick increase in temperatures higher than 850°C that correspondingly reveals in DTA curve shifting to the exothermic peak. The fractional conversion evaluated by considering the weight increase up to 1000°C in TG corresponding to the oxidation reaction of Ti-6Al-4V-xB$_4$C to Al_2O_3 was nearby 6% and 21%, in that order. The oxidation nature of a Ti-6Al-4V-xB$_4$C to the fractional transformation of 8% gives the impression to hint at the formation of amorphous or poorly crystallized Al. The oxidation of Ti-6Al-4V-B$_4$C takes in the formation of intermediate oxides at temperatures as low as 600°C. In dissimilarity with such a lower reactivity of Ti-6Al-4V-xB$_4$C, the oxidation carry on at a more rapid rate at temperatures beyond 850°C and achieved the higher fractional conversion of 21% at 1000°C.

The oxygen transference influencing the oxidation frequency of the coating and initial range of activation energy is the most important dispute to initiate oxidization. At first thermal energy for initial oxidation is sufficient to support the diffusion of oxygen atoms towards the coating surface, and as a result formation of Ti rich region in the coating surface as well as the formation of TiO_2 identified; it happens mainly because of oxygen contents close to the coating surface region. Suddenly, the diffusion of Ti and Al ions with atomic oxygen towards the inside coating will form a (TiO_2, Al_2O_3) layer on the coating surface, which may be performing as an active diffusion barrier and down the inside diffusion of the oxygen. In continuation, the amorphous oxide thin layer was transformed into a crystalline phase by increasing the temperature up to the limit of 600°C. On the other hand, by increasing the temperature range up to 700°C, the diffusion tracks were destroyed by the

influence of the oxidation process so that the rate of oxidation was reduced. By way of increasing the temperature due to the expansion of melted aluminium (in 660°C), it created an intense tension on the crust. In the interior, the temperature range of 800-900°C, the melt ruptured the crust and saturated outward. The interaction of this melt with an oxide atmosphere created intense oxidation. Additionally, according to the presence of the aluminium leftover in the products, it may be inferred that the whole oxidization method failed to turn up even up to 1000°C.

3.4. Nanohardness

Nanohardness of Ti-6Al-4V-2ZrC thin film coatings are calculated by the AFM nanoindentation technique. An AFM image is obtained through the contact mode AFM procedure and depth of penetration during indentation is deliberate from the same image. For the period of indentation, a force-displacement (F-D) curve is secured in addition to nanohardness and is evaluated from the relevant F-D curve. The maximum of 4 *nN* load is applied, and after putting on the mentioned load, the tip penetrates without obstruction to the Ti-6Al-4V-2ZrC coating that is brought to light by way of the blue inclined stripe. At that moment, the tip is standing a little apart with coating. The nanohardness is calculated by the indentation load divided by the projected contact area by using Equation (8) (Kailasanathan & Selvakumar, 2012).

$$H = \frac{P}{24.5(h_c)^2} \tag{8}$$

where–P - maximum applied load, –c - penetration depth.

The nanoindentation force-displacement curve of the different coating is shown in Fig. 6 (a-e). The indentation depth of the thin film coating controls the hardness values of the Ti-6Al-4V-xB_4C coated AISI 1040 steel substrate. The contribution of the underlying softer substrate with Ti-6Al-4V-xB_4C coating became more evident with higher hardness. In five coatings, all data exhibits that most amazing hardness values are around 14.9 *GPa*. With the increasing B_4C content, the hardness starts to increase because of substrate effects. Fig. 6 (a-e) demonstrates the variation in nanohardness of Ti-6Al-4V-xB_4C coating. Constant substrate temperature was maintained during the coating time and hardness of the Ti-6Al-4V-xB_4C composite coatings was increased because of the increase of B_4C particles. This is because of the B_4C content in the coating that concedes the development of coarse structures which prompts the increase of the nanohardness. The higher nanohardness of Ti-6Al-4V-xB_4C coatings occurs because of the better surface topography and homogeneously dispersion of nano B_4C particles in the coating.

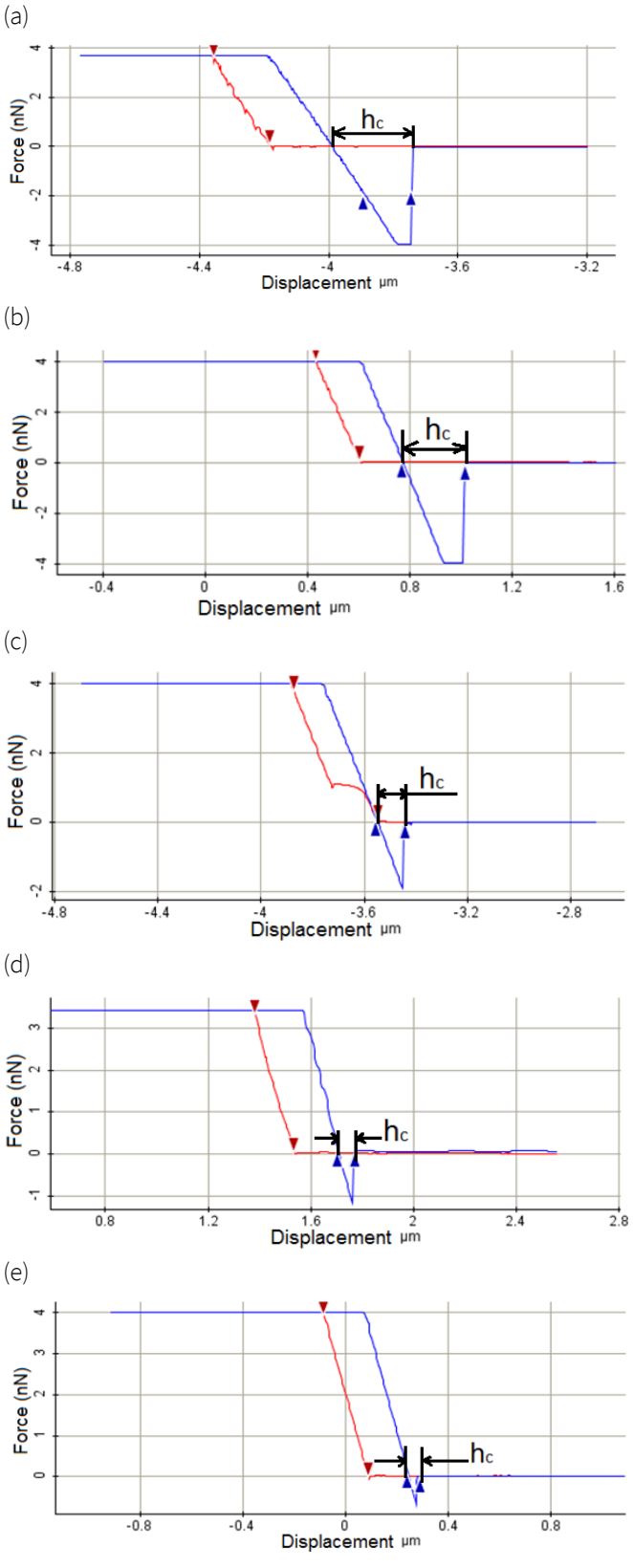

Figure 6. Force-depth curves of nanoindentation test for Ti-6Al-4V-xB_4C coatings with different B_4C (%) (a) x=0, (b) x=2, (c) x=4, (d) x=6, (e) x=8.

Fig. 7 shows the nanohardness comparison of Ti-6Al-4V-xB_4C coating with varying B_4C %. The nanohardness was increased for higher B_4C content as well as stable substrate temperature. In addition, it is recorded that the nanohardness was increased with an increase in the percentage of B_4C particles. Due to the formation of more B_4C particles in the coating which acknowledges the formation of coarse structures which increases the nanohardness. However, at higher B4C contents, nanohardness of the Ti-6Al-4V-xB_4C thin layers increases, moreover it is clearly stated that nanohardness of the Ti-6Al-4V-xB_4C coating increases with an increase in the amount of B_4C reinforcement. The higher nanohardness of Ti-6Al-4V-xB_4C thin film coatings is caused by the finer surface topography, high dense structure in addition to the homogeneous dispersal of B_4C particles in the coating.

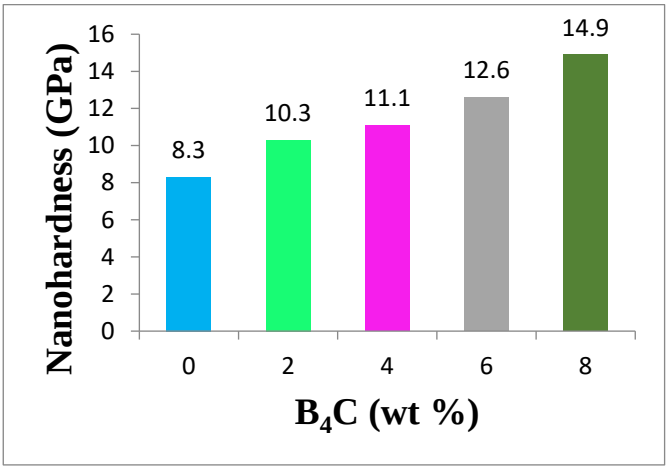

Figure 7. Nanohardness of Ti-6Al-4V-B_4C coatings with different % of B_4C.

3.4.1. Strengthening of Ti-6Al-4V-B4C coatings

High surface energy and a smaller size of particles in the coating were developed into a cluster of particles and generated bunches in the coating. During the deposition process, some of the nano B_4C particles were clustered and the size of the cluster was around 100 nanometers. The higher volume of B_4C particles focus would build the amount of particles suspended inside the coating, prompting extra particles amalgamated into the coatings that progressively improved the strengthening outcome by extra phase dispersion. The nano-particles on the coated surface would play out the piece of nucleation sites just as dealing with the grain developing. In this way, a decrease in the grain size of the coatings additionally ended up with grain refinement strengthening. On the other hand, by increasing the quantity of B_4C in the coating, a higher number of particle clusters was identified. Further B_4C clusters were embedded into the Ti-6Al-4V-xB_4C coating, prompting poor particle dispersion to bring about expansion to uniform porous structure. Therefore, the reinforcing result by B_4C particles distribution was confined by the challenge of the on top of 2 mechanisms. Significant improvement of the mechanical properties of the coating occurred by an imperial dispersion strengthening mechanism and grain refinement during coating. Moreover, the B_4C particles in the coating refined the grain size of the Ti-6Al-4V-xB_4C coatings because of its smaller particle size. Furthermore, discussing the indication of dispersion strengthening was acknowledged by a dispersed additional phase microstructure. On an outset, high nanohardness was achieved because of a highly dispersed microstructure. The reduction in grain size of the particles produced additional grain boundaries surface of the coating which increased the surface hardness of the coating reported by Musil (2012).

4. Conclusions

The results are summarized as follows:

- Microstructure studies show that the B_4C particles were scattered uniformly in the coating and they were characterized by SEM, AFM and XRD.
- The ignition period of the coating was increased because of the addition of B_4C confirmed by TG/DTA. The amount of B_4C in the coating has an emotional impact on the change of enthalpy for the period of decomposition.
- The DTA result entails a rapid phase transition of coating, as a result, mass loss occurs throughout the decomposition at the sooner stage. Supplementary, it was that in decomposition, the transformation of enthalpy affects by a quantity of B_4C presence within the coating.
- TiO_2, Al_2O_3, V_2O_5 and B_2O_3 layers were identified on the coating surface to the diffusion of Ti, Al, V and B4C ions with oxygen particles. The oxidization rate of the coating was controlled by oxygen content transference. The activation energy of coating is the key factor to initiate oxidization in the coating.
- The oxidation behaviour of Ti-6Al-4V-B_4C coatings was implemented at different stages. A very negligible oxidation rate was identified at the initial stage. By raising the temperature level up to 600°C, the amorphous oxide crust was transformed into the crystalline phase. But, with more temperature rising up to 700°C, the diffusion tracks were damaged by the influence of the oxidization method in order that the speed of oxidization was reduced.
- The inclusions of B_4C particles into the coating enhance the nanohardness.

References

An, T., Wen, M., Hu, C Q., Tian, H. W., Zheng, W. T. (2008). Interfacial fracture for TiN/SiNx nano-multilayer coatings on Si (1 1 1) characterized by nanoindentation experiments. *Materials Science & Engineering A,* 494, 324–328. https://doi.org/10.1016/j.msea.2008.04.020

Azhagurajan, A., Selvakumar, N., Mohammed Yasin, M. (2012). Minimum ignition energy for micro and nano flash powders. *Process Safety Progress, 31*(1), 19–23. https://doi.org/10.1002/prs.10503

Belmonte, M. (2006). Advanced Ceramic Materials for High Temperature Applications. *Advanced Ceramic Materials, 8,* 693-703. https://doi.org/10.1002/adem.200500269

Chavin Jongwannasiri., Xianghui Li., Shuichi Watanabe. (2013). Improvement of thermal stability and tribological performance of Diamond-Like Carbon composite thin films. *Materials Sciences and Applications, 4,* 630-636. https://doi.org/10.4236/msa.2013.410077

Kailasanathan, C., & Selvakumar, N. (2012). Comparative study of hydroxyapatite/gelatin composites reinforced with bio-inert ceramic particles. *Ceramics International, 38*(5), 3569-3582. https://doi.org/ 10.1016/j.ceramint.2011.12.073

Lin, J., Mishra, B, Moore, J. J., Sproul, W. D. (2008). A study of the oxidation behavior of CrN and CrAlN thin films in air using DSC and TGA analyses. *Surface and Coatings Technology, 202*(14), 3272–3283. https://doi.org/10.1016/j.surfcoat.2007.11.037

Musil, J. (2012). Hard nanocomposite coatings: Thermal stability, oxidation resistance and toughness. *Surface and Coatings Technology,* 207, 50-65. https://doi.org/10.1016/j.surfcoat.2012.05.073

Polyakova, I. G., & Hübert, T. (2001). Thermal stability of TiN thin films investigated by DTG/DTA. *Surface and Coatings Technology, 141*(1), 55-61. https://doi.org/10.1016/S0257-8972(01)01042-8

Prince, R. M. R., Selvakumar, N., Arulkirubakaran, D., Sreedharan, C. E. S., Thulasiram, R., & Kumar, R. M. (2020). Surface structural features and wear analysis of a multilayer Ti6Al4V-B 4 C thin film coated AISI 1040 steel. *Materials Research Express.* 7(1), 016436 https://doi.org/10.1088/2053-1591/ab6c18

Padture, N. P., Gell, M., & Jordan, E. H. (2002). Thermal barrier coatings for gas-turbine engine applications. *Science,* 296, 280-284. https://doi.org/ 10.1126/science.1068609

Robinson, G. M., Jackson, M. J. (2005). A review of micro and nanomachining from a materials perspective. *Journal of Material Processing Technology,* 167, 316–37. https://doi.org/10.1016/j.jmatprotec.2005.06.016

Selvakumar, N., & Prince, R. (2017). Microstructure, surface topography and sliding wear behaviour of titanium based coating on AISI 1040 steel by Magnetron Sputtering. *Archives of Civil and Mechanical Engineering,* 17, 281-292. https://doi.org/10.1016/j.acme.2016.10.005

Selvakumar. N., Sivaraj, M., Muthuraman, S. (2016). Microstructure characterization and thermal properties of Al-TiC sintered nano composites. *Applied Thermal Engineering,* 107, 625–632. https://doi.org/10.1016/j.applthermaleng.2016.07.005

Selvakumar, N., & Vettivel, S. C. (2013). Thermal, electrical and wear behavior of sintered Cu–W nanocomposite. *Materials & Design*, 46, 16-25. https://doi.org/10.1016/j.matdes.2012.09.055

Shimada, S., Johnsson, M., & Urbonaite, S. (2004). Thermoanalytical study on oxidation of TaC1− xNx powders by simultaneous TG-DTA-MS technique. *Thermochimica acta, 419*(1-2), 143-148. https://doi.org/10.1016/j.tca.2004.02.009

Stecura, S. (1986) Optimization of the Ni-Cr-Al-Y/ZrO2-Y2O3 thermal barrier system. *Advanced Ceramic Materials, 1,* 68-76.

Yang, Y. S., Cho, T. P., & Lin, Y. C. (2014). Effect of coating architectures on the wear and hydrophobic properties of Al–N/Cr–N multilayer coatings. *Surface and Coatings Technology,* 259, 172–177. https://doi.org/10.1016/j.surfcoat.2014.01.058